Journal of Fluids and Structures (1998) **12,** 631–654
Article No. fl980163

ANALYSIS OF FLUID–STRUCTURE INTERACTIONS USING A TIME-MARCHING TECHNIQUE

I. JADIC†, R. M. C. SO§ and M. P. MIGNOLET†

† *Mechanical and Aerospace Engineering, Arizona State University*
Tempe, AZ 85287-6106, U.S.A.
§ *Mechanical Engineering, The Hong Kong Polytechnic University*
Hung Hom, Kowloon, Hong Kong

(Received 31 August 1997 and in revised form 3 April 1998)

Fluid–structure interaction problems arise in many different areas of engineering where the system considered or some of its components are directly in contact with a fluid. Examples are aircraft, jet engines, ships, pipelines, nuclear and chemical reactors, offshore structures, bridges, etc. In these cases, the fluid often plays an important role in determining the behavior of the structure of interest. For example, flutter could have disastrous consequences on aircraft, and resonances resulting from flow-induced vibrations could provoke structural failures in nuclear reactors, bridges and other structures subjected to a cross-flow. To prevent these potential dramatic and expensive accidents, it is necessary to seek a reliable technique for the determination of the characteristics, in particular natural frequencies, damping levels and fatigue life, of the structure in the presence of the fluid. This computation has often been accomplished in the past by relying on either a total or substantial decoupling of the fluid and structural problems, but the ever increasing emphasis on reliability, efficiency, and weight motivates the use of precise strategies for the determination of the fluid and structural behaviour. Recent efforts in this area indicate that a time-marching solution for the combined fluid and structure governing equations is computationally feasible and may provide the necessary accuracy. The present investigation essentially verifies this approach and makes available a time-marching technique that fully resolves the fluid–structure interactions. As an illustration, the single airfoil flutter problem is first analysed in detail. This is followed by an investigation of the nonlinearity in the response of the airfoil. New insights thus obtained are presented and discussed.

1. INTRODUCTION

THE ACCURATE PREDICTION OF FLOW-INDUCED VIBRATIONS in turbomachines is one of the most important and challenging problems in the area of fluid–structure interactions. The complex geometry of the bladed disks, the effects associated with the rotation of the rotors, and the cascade structure of each rotor–stator stage are only some of the difficulties encountered. This situation has quite naturally led to the introduction of simplifying assumptions. In particular, the fluid forces on the blades have often been split into two contributions (Chiang & Kielb 1993): the motion-dependent unsteady aerodynamic forces and the gust-response unsteady aerodynamic forces. The forces belonging to the first group are directly related to the structural deformations and modify the structural (no flow) mass, damping, and stiffness matrices. They are considered in both the free vibration/flutter speed determination and forced vibration problems. The forces that are in the second group model the flow deflects that are associated with inlet distortions, wake disturbances (from upstream stages), or potential disturbances. It is often assumed that these forces are

0889–9746/98/060631 + 24 $30.00

not coupled with the structural deformations so that they can be considered as an external excitation to the combined fluid–structure system, i.e. as a travelling vortical gust. In particular, models of the wakes of an upstream stage have been considered as a gust convected with the mean flow ("frozen gust"), with a profile that is either fixed (Fleeter 1994; Weaver & Fleeter 1994) or changing in a predetermined manner (Kemp & Sears 1955; Majjigi & Gliebe 1984) to account, in particular, for the presence of the blades.

In this light, the primary goal of this investigation is to develop a simple, modular time-marching strategy that accounts for the *full* fluid–structure interaction for both the free vibration/flutter speed determination and forced vibration problems, including the estimation of the fatigue life of the structure. Although some of the components of the formulation may not be adequate in all situations, e.g. the aerodynamic computations rely on the assumption of an attached flow, they can easily be replaced by more appropriate prediction tools for the application considered. The interaction between a turbomachine blade row and the passing fluid will be used to exemplify the approach as well as to illustrate some of the shortcomings of the aforementioned modelling of wakes shed by upstream stages as vortical gusts.

This paper is the first of a series of reports on this subject, and it concentrates on the development of a time-marching technique where the full fluid–structure interaction effects are investigated. In order to demonstrate the viability of such a technique, the flutter problem treated by Hall (1994) is used as a benchmark to verify the present technique. In the process, it is shown that nonlinear effects that arise from interactions between the flow, the wake and the airfoil are present in the problem and that their neglect may not be justified in the context of a true fluid–structure interaction problem. It will also be shown that these small nonlinear effects are not easily resolved if an accurate and reliable data analysis technique of time series is not available. The development of such a data analysis technique is crucial to the successful development of a comprehensive method for the analysis of fluid–structure interaction problems, including flutter. Once verified, the technique can be used to analyse a host of flow-induced vibration problems, such as blade vibrations in turbomachines, and the assessment of their potential for failure. Subsequent tasks of the present research will be reported in separate papers.

2. TIME-MARCHING FORMULATION

The analysis of flow-induced vibration problems by time-marching strategies requires (i) the modeling of the fluid, (ii) the prediction of the dynamic response of the structure, (iii) the specification of the coupling between the fluid and the structure, (iv) the frequency domain analysis of the response time histories, and (v) the assessment of the potential for failure. All of these elements or modules must be included in the solution technique and each one of them must be selected according to the specific application considered. The focus of the present investigation on subsonic turbomachines has led to the formulation of these five components. However, only the first four are briefly discussed below. The fifth will be discussed in detail in a subsequent paper.

2.1. Aerodynamic Modelling

The starting point of this analysis is the time-averaged Reynolds mean flow equations. In writing down the governing equations, the flow is assumed to be incompressible, two-dimensional and unsteady. Furthermore, turbulent diffusion is considered to be significantly larger than molecular diffusion. Therefore, to the lowest order, the effect of molecular

diffusion can be neglected. If a constant eddy viscosity v_t is assumed, the Reynolds equations are identical to the Navier–Stokes equations. The equations can then be normalized using the reference velocity, U_∞, and the chord length, c, so that the Reynolds number, Re_t is given by $U_\infty c/v_t$. Thus simplified, the governing equations can be written as

$$\nabla \cdot \mathbf{V} = 0. \tag{1}$$

$$\frac{\partial \mathbf{V}}{\partial t} + \mathbf{V} \cdot \nabla \mathbf{V} = -\nabla P + \mathrm{Re}_t^{-1} \nabla^2 \mathbf{V}, \tag{2}$$

where $\mathbf{V}$ is the mean dimensionless velocity vector, P is the mean dimensionless pressure, t is the dimensionless time and $\mathrm{Re}_t = U_\infty c/v_t$ is the Reynolds number based on the eddy viscosity v_t. The oncoming flow is considered to be either a uniform shear flow or a uniform flow with constant vorticity. Since the former can also be reduced to an equivalent uniform flow with constant vorticity, the reference velocity U_∞ can be taken as the uniform flow velocity without loss of generality. In writing the governing equations in this form, it has been tacitly assumed that the eddy viscosity is constant for both the oncoming flow and the free vortex. The constant eddy viscosity assumption for the free stream is justified because in a two-dimensional near-homogeneous turbulent flow, v_t is approximately constant (Batchelor 1953). In anticipation of the fact that, following Chorin (1973), the method of fractional steps is used to handle the governing equations, it is reasonable to assume v_t in the vortex, to the lowest order, to be approximately constant also. The rationale for this assumption is detailed below.

The mean pressure P can be eliminated by taking the curl of equation (2). Since the mean vorticity is defined by $\boldsymbol{\omega} = \nabla \times \mathbf{V}$, an equation governing the transport of $\boldsymbol{\omega}$ is given by

$$\frac{\partial \boldsymbol{\omega}}{\partial t} + \mathbf{V} \cdot \nabla \boldsymbol{\omega} = \mathrm{Re}_t^{-1} \nabla^2 \boldsymbol{\omega}. \tag{3}$$

The oncoming flow is two-dimensional and can be assumed to be made up of three components superimposed on each other; a uniform flow, a piecewise continuous distribution of vorticity (typical of that generated by a uniform shear) and concentrated vortices. In a two-dimensional flow, the vorticity $\boldsymbol{\omega}$ is perpendicular to the plane of the flow. This observation applies not only to a continuous distribution of vorticity, but also to a concentrated one. In both cases, the vorticity can be represented by infinite filaments perpendicular to the two-dimensional plane flow. If the circulation Γ is defined as

$$\Gamma = \oint \mathbf{V} \cdot \mathrm{d}\mathbf{l}, \tag{4}$$

where the integral is taken around a closed material curve drawn in the fluid, an integral formula equivalent to equation (3) can be obtained (Batchelor 1967),

$$\frac{\partial \Gamma}{\partial t} = -\nu \oint (\nabla \times \boldsymbol{\omega}) \cdot \mathrm{d}\mathbf{l}. \tag{5}$$

For an inviscid flow, equation (5) reduces to $\partial \Gamma/\partial t = 0$. This is Kelvin's theorem and simply states that Γ around any material closed curve in the flow field does not change with time.

In this study, the main interest is in the influence of an upstream source of vorticity, which is approximated by a concentrated "travelling" vortex or by a series of vortices, on a downstream blade (isolated or in a cascade). The mechanism of vorticity generation and dissipation, given by the terms on the right-hand side of equations (3) and (5), is of somewhat lesser importance than the convection of vorticity. Thus, the decoupling of the convection and dissipative aspects proposed by Chorin (1973) could be used to handle equations (3) and (5). According to this decoupling technique, the circulation Γ around a given material curve remains unchanged during a small time step δt (fractional time step). Furthermore, it is assumed that, during this time step δt, the flow behaves like an inviscid "conveyor" of the vorticity thus "frozen". Once this time step is consumed, the vorticity is altered by diffusion. In mathematical terms, this can be written as

$$\mathbf{x}_{vi}(t + \delta t) = \mathbf{x}_{vi}(t) + \mathbf{V}_o(\mathbf{x}_{vi}(t), \omega_i(t), t)\delta t, \quad i = 1, 2, \ldots, N, \tag{6}$$

where $\omega_i(t) = f(t)$ is the strength of the ith vortical element, $\mathbf{x}_{vi}$ is the position vector of the ith vortical element, N is the number of vortical elements, and $f(t)$ is a known function which governs vortex diffusion. The suffix "o" attached to the velocity $\mathbf{V}$ emphasizes the fact that the convective velocity is generated by an inviscid flow. The set of equations (6) is in fact an explicit finite difference form of the differential set of equations which relate the position of a certain vortical element to the velocity of the inviscid flow at that particular location. In this investigation Lamb's (1932) viscous core model is used to approximate $f(t)$:

$$|\mathbf{V}| = \frac{\Gamma_v}{2\pi}\frac{1}{r}\left[1 - \exp\left(\frac{r^2}{4t}\,\mathrm{Re}_t\right)\right],$$

where Γ_v is the strength of the vortex.

Consistent with the above discussion, the method of fractional steps (Chorin 1973) is now used to split (3) into the following set:

$$\frac{\mathrm{d}\omega_c}{\mathrm{d}t} = \frac{\partial\omega_c}{\partial t} + \mathbf{V}\cdot\nabla\omega_c = 0, \tag{7a}$$

$$\frac{\partial\omega_d}{\partial t} = \mathrm{Re}_t^{-1}\nabla^2\omega_c, \tag{7b}$$

where ω_c and ω_d are the convective and diffusive part of the vorticity, respectively. It follows that ω_d is the approximate solution to equation (3). In other words, the path of the vortex is solely determined by equation (7a) while the diffusion of the vortex is obtained by solving equation (7b). Therefore, in this treatment, vortex diffusion is assumed to have little effect on its path. In view of this, it is reasonable to assume v_t in the vortex, to the lowest order, to be approximately constant.

The flow around the structure, which is simulated by a distribution of sources and discrete vortices, is solved using a Boundary Element Method for inviscid incompressible flow. The boundary condition requires the flow to be tangent to the surface of the structure. The far-field boundary condition is given by $\mathbf{V}_o = \mathbf{V}_\infty + \mathbf{V}_\omega$, where $\mathbf{V}_\omega$ is the rotational part of $\mathbf{V}_o$. In this study U_∞ is taken to be the magnitude of $\mathbf{V}_\infty$. Solving the given boundary equations yields the source and vorticity distributions on the structure surface. Then, successively, the flowfield velocities and pressure distributions are calculated. Further details concerning this formulation can be found in Yao *et al.* (1989, 1995) and Yao & Liu (1994). Once the unsteady velocity, $\mathbf{V}$, and unsteady pressure, p, fields are known, the unsteady forces on the structure can be determined.

2.2. Structural Dynamic Modelling

The dynamic response of structures is in general governed by a set of partial differential equations, wherever the mass is continuously distributed, and/or ordinary differential equations that describe the behaviour of lumped masses. Although these equations are often assumed to be linear, nonlinear terms can appear due to geometric factors (large rotations, intermittent contact of shrouds, etc.) or to the material properties of the structures (large deformations, nonelastic behaviour).

In the context of airfoils and turbomachine blades, the simple two-degree-of-freedom structural model shown in Figure 1 has often been assumed. Since the objective is to develop a technique to analyse fluid–structure interactions, there is no loss of generality in starting with an accepted simple structural model. The modelled equations of motion are:

$$m\ddot{h} - ma\cos\theta\ \ddot{\theta} + k_h h + ma\sin\theta\ \dot{\theta}^2 = L, \tag{8a}$$

$$I\ddot{\theta} - ma\cos\theta\ \ddot{h} + k_\theta\theta = M, \tag{8b}$$

where h is the plunging displacement of the blade, which models the bending deformation, and θ is the pitching angle of the blade, which is representative of torsional deformation. The coefficient a is the distance between the elastic axis and the center of mass, m is the mass of the blade section with a unit spanwise length, I is the moment of inertia of the blade section, k_h and k_θ are the bending and torsional stiffnesses, respectively, and L and M are the aerodynamic lift and moment acting on the blade. In general, (8a) and (8b) are nonlinear. However, in anticipation of the fact that a linear counterpart of (8) will be solved later, their linearized version is also included here for reference. The corresponding linear version is

$$m\ddot{h} - ma\ddot{\theta} + k_h h = L, \tag{9a}$$

$$I\ddot{\theta} - ma\ddot{h} + k_\theta\theta = M. \tag{9b}$$

Furthermore, consistent with the linear assumption made to deduce (9a, b) the L and M on the right-hand side of (9a, b) should also be linearized. Their linearized forms are given in the following.

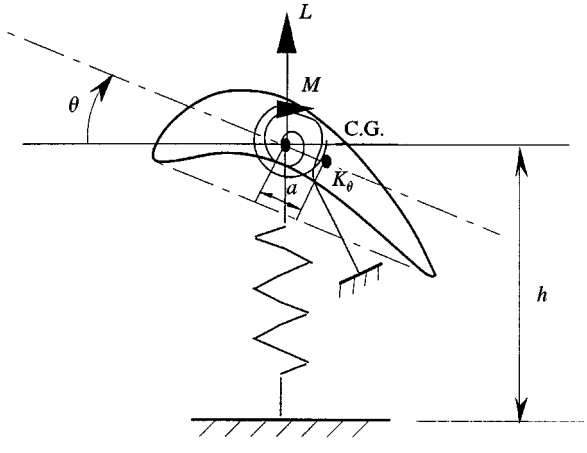

Figure 1. Structural dynamics model.

2.3. Fluid-Structure Coupling

The flow field and the structural response are coupled to each other through the tangency boundary condition (effect of structural response on the flow field) and the aerodynamic forces (effect of the flow field on the structural response). Specifically, for the inviscid flow considered here, the flow field is required to satisfy, at every point of the surface of the structure in contact with the fluid, the tangency condition

$$(\mathbf{V}_o - \mathbf{V}_S) \cdot \mathbf{n} = 0, \tag{10}$$

where $\mathbf{V}_o$ and $\mathbf{V}_S$ are the local velocities of the fluid and the structure, and $\mathbf{n}$ is the local normal to the contact surface. Note that this boundary condition is in general nonlinear since both the velocities and the direction of the normal depend on either the flow field variables (e.g., strengths and locations of the vortices) or the structural response.

In the structural modelling considered here, the flow field affects the structural response through the aerodynamic forces L and M in equation (9), which can be evaluated from the pressure distribution,

$$C_p = \frac{2(p - p_\infty)}{\rho U_\infty^2} = \frac{1}{U_\infty^2}\left[- 2\frac{\partial \phi}{\partial t} + V_R^2 \right], \tag{11}$$

where p is the unsteady pressure on the blade surface, p_∞ is the reference pressure, ρ is the fluid density, ϕ is the velocity potential, $\mathbf{V}_R$ is the resultant blade surface velocity taking into account all contributions including the freestream velocity, the blade motion, the velocity induced by the source and vorticity distributions, the travelling and the wake vortices. Once p is known, the L and M can be determined by integrating p around the surface of the airfoil. A lift and moment coefficient, C_L and C_M, can be calculated from the following relations:

$$C_L = \frac{L}{(\frac{1}{2})\rho U_\infty^2 c} = -\oint [-C_p(s) n_x(s) \sin\alpha + C_p(s) n_y(s) \cos\alpha]\, \mathrm{d}s, \tag{12}$$

$$C_M = \frac{M}{(\frac{1}{2})\rho U_\infty^2 c^2} = \oint \{[x(s) - x_P] C_p(s)\, n_y(s) - [y(s) - y_P] C_p(s) n_x(s)\}\, \mathrm{d}s, \tag{13}$$

where s is the arc length of the blade surface contour, n_x, n_y are the x, y components of the outward normal unit vector on the blade surface, respectively, x_P and y_P are the coordinates of the blade mass center, and α is the angle of attack. The corresponding linear version is

$$C_L = -\oint [-C_p(s) n_x(s) \alpha + C_p(s) n_y(s)]\, \mathrm{d}s, \tag{14}$$

$$C_M = \oint [x(s) - x_P]\, C_p(s) n_y(s)\, \mathrm{d}s. \tag{15}$$

2.4. Time History Analysis

The direct result of the application of a time-marching strategy to a fluid–structure interaction problem is a series of time histories of the evolution of the fluid flow characteristics, such as strengths of vortices, forces on the structure, and of the structural responses. Although some of the failure criteria that can be considered are expressed in terms of the values of the response, e.g. failure occurs when a displacement or stress exceeds a specified

threshold, many of them are formulated in terms of the frequency domain aspects of the response. Flutter and fatigue are failure mechanisms that fall in this second category, flutter occurs when a purely harmonic, undamped response of the structure arises from its interaction with the fluid, while fatigue is based on the damage generated by each harmonic component present in the time histories of the stresses.

Classically, the transition from the time domain to the frequency domain has been accomplished by relying on the fast fourier transform (FFT) technique. However, this procedure has a serious shortcoming when considering its application to the determination of the flutter speed and to the estimation of the fatigue life of lightly damped structures. The difficulty lies in the intimate relation between the resolution of the FFT and the number of points available in the time series. If n_r denotes the number of available samples of a specific variable and Δt is the sampling time interval, then the FFT method will yield n_r frequency response estimates in the domain $[-1/2\Delta t, 1/2\Delta t]$ so that its resolution is equal to $\Delta f = (1/n_r \Delta t)$ Hz. However, most modern structures are very lightly damped, even in the presence of the fluid, so that their frequency response functions (or transfer functions) exhibit extremely sharp peaks centered at the natural frequencies f_i and of bandwidths of the order of $2\zeta_i f_i$, where ζ_i is the associated damping ratio, typically of the order of 0·01 or less. Since it is the frequency content of the response within these small bands that dictates the fatigue life of the structure, it is necessary to select $\Delta f \ll 2\zeta_i f_i$, say $\Delta f \approx (2\zeta_i f_i)/6$, to obtain an accurate estimate of the damage created in the ith mode. The value of the sampling time Δt is often prescribed by the physics of the problem to be less than a certain limit. On the other hand, the condition $\Delta f \approx (2\zeta_i f_i)/6$ requires a long time history of the response. In the context of a time-marching solution of the coupled fluid–structure governing equations, long records imply a tremendously large computational effort. A similar situation is encountered in connection with the determination of the flutter speed which occurs when the damping ratio in one mode of the combined fluid–structure system equals zero.

To circumvent these difficulties, an alternative approach based on autoregressive moving average (ARMA) discrete models (Marple 1987; Mignolet & Red-Horse 1994) that have been used for the evaluation of the frequency characteristics of vibrating structures, is considered. In developing the ARMA identification/spectral estimation technique, it is convenient to first consider a linear multi-degree-of-freedom dynamic model of the form (it will be shown later that nonlinearities are also readily accounted for).

$$\mathbf{M}_{\mathrm{st}}\ddot{\mathbf{X}}_{\mathrm{st}}(t) + \mathbf{K}_{\mathrm{st}}\mathbf{X}_{\mathrm{st}}(t) = \mathbf{F}(t), \tag{16}$$

where $\mathbf{X}_{\mathrm{st}}(t)$, $\mathbf{M}_{\mathrm{st}}$ and $\mathbf{K}_{\mathrm{st}}$ denote the time-dependent vector of the structure, and its mass and stiffness matrices, respectively. Then, it can be shown that the sampled response vector $\tilde{\mathbf{X}}_n = \tilde{\mathbf{X}}_{\mathrm{st}}(n\Delta t)$ admits the representation (Mignolet & Red-Horse 1994)

$$\tilde{\mathbf{X}}_n = -\sum_{k=1}^{s} \tilde{A}_k \tilde{\mathbf{X}}_{n-k} + \sum_{k=0}^{s-1} \tilde{B}_k \tilde{\mathbf{F}}_{n-k} + \sum_{k=0}^{s} \tilde{C}_k \tilde{\mathbf{W}}_{n-k}, \tag{17}$$

where

$$\tilde{\mathbf{X}}_n = \tilde{\mathbf{X}}_{\mathrm{st}}(n\,\Delta t) \quad \text{and} \quad \tilde{\mathbf{F}}_n = \tilde{\mathbf{F}}_{\mathrm{st}}(n\,\Delta t), \quad n = 1, 2, 3, \ldots \tag{18}$$

are the noise (computational inaccuracies/measurement errors) corrupted values of the response and excitation time histories, respectively, and $\tilde{\mathbf{W}}_n$ is a noise vector. In the present analysis, the system includes the structural variables (h and θ of the blade) and the aerodynamic degrees of freedom, which are not directly observed. Note that this combined

fluid–solid system is not subjected to any external excitation, so that the second term on the right-hand side of equation (17) disappears. Finally, since the only source of error lies in numerical inaccuracies, this relation could be further simplified by just considering the first term in the last sum. The result is

$$\tilde{\mathbf{X}}_n = -\sum_{k=1}^{s} \tilde{A}_k \tilde{\mathbf{X}}_{n-k} + \tilde{C}_0 \tilde{\mathbf{W}}_n, \tag{19}$$

which represents a purely autoregressive (AR) model. The parameter $s = 2(N_{\text{aero}+\text{st}})/d$ where $N_{\text{aero}+\text{st}}$ is the total number of aerodynamic and structural degrees of freedom and d is the number of observed degrees of freedom. Here, $d = 2$ if only the structural responses h and θ are observed or $d = 4$ if, in addition to these variables, the values of the aerodynamic coefficients C_L and C_M are also considered.

The ARMA spectral estimation/identification technique requires first the determination of the matrix coefficients $\tilde{A}_k$ and $\tilde{C}_0$ that yields a "best" fit of the computed time series $h(t)$ and $\theta(t)$. This is achieved by maximizing the likelihood function of the observed time series (Mignolet & Red-Horse 1994). This condition yields under the assumption of a Gaussian distribution of the noise samples $\tilde{\mathbf{W}}_n$ the following linear set of algebraic equations for the parameters $\tilde{A}_k$ and $\tilde{C}_0$:

$$\sum_{k=1}^{s} \tilde{A}_k R_{xx}(k-r) = R_{xx}^{\mathrm{T}}(r), \quad r = 1, 2, \ldots, 3, \tag{20}$$

where $(\ )^{\mathrm{T}}$ denotes the transpose of a matrix and

$$R_{xx}(0) + \sum_{k=1}^{s} \tilde{A}_k R_{xx}(k) = \frac{2\pi}{\Delta t} \tilde{C}_0 \tilde{C}_0^{\mathrm{T}}. \tag{21}$$

Note in the above relation that, for simplicity and without loss of generality, the matrix $\tilde{C}_0$ can be assumed to be lower triangular so that it is obtained by the Cholesky decomposition of the left-hand-side term. Further, the correlation matrix function $R_{xx}(k)$ can be evaluated as

$$R_{xx}(k) = \frac{1}{N_{\text{sam}}} \sum_n \tilde{X}_{n-k} \tilde{X}_n^{\mathrm{T}}, \tag{22}$$

where N_{sam} is the total number of samples in the time histories of the response $\tilde{X}_n$ and the summation over n extends over all available samples. Once the model parameters $\tilde{A}_k$ and $\tilde{C}_0$ have been computed, the spectral matrix of $\tilde{X}_n$ can be estimated for any frequency ω as

$$S_{xx}(\omega) = \left(\mathbf{I}_d + \sum_{k=1}^{s} \tilde{A}_k \mathrm{e}^{\mathrm{i}\omega k \Delta t} \right)^{-1} \tilde{C}_0 \tilde{C}_0^{\mathrm{T}} \left(\mathbf{I}_d + \sum_{k=1}^{s} \tilde{A}_k^{\mathrm{T}} \mathrm{e}^{-\mathrm{i}\omega k \Delta t} \right)^{-\mathrm{T}}, \tag{23}$$

where $\mathbf{I}_d$ is the $d \times d$ identity matrix.

The above autoregressive modelling can also be used in connection with experimental data provided that the signal-to-noise ratio is sufficiently large to consider only one term in the last sum appearing in equation (17). In the negative, a full ARMA modelling strategy that leads to a nonlinear algebraic set of equations for the matrix parameters $\tilde{A}_k$ and $\tilde{C}_0$ must be used. The solution of this nonlinear algebraic set of equations can be obtained in a series of linear steps [see Mignolet & Red-Horse (1994) for a complete presentation].

In the context of both AR and ARMA models, it has been shown (Mignolet & Red-Horse 1994) that the roots z_l of the equation

$$\det\left(\mathbf{I}_d + \sum_{k=1}^{s} \tilde{A}_k z_l^{-k}\right) = 0, \tag{24}$$

are related to the natural frequencies ω_l and the damping ratios ζ_l of the system, as

$$\omega_l = \frac{1}{\Delta t}|\ln z_l| \quad \text{and} \quad \zeta_l = -\frac{1}{\omega_l}\ln|z_l|. \tag{25}$$

The mode shapes can also be computed from the parameters $\tilde{A}_k$. Specifically, the lth mode shape is proportional to the eigenvector of the complex matrix $I_d + \sum_{k=1}^{s} \tilde{A}_k z_l^{-k}$ corresponding to its zero eigenvalue (Mignolet & Red-Horse 1994).

The knowledge of the natural frequencies, damping ratios and mode shapes of the different modes present in the response of the system allows the determination of the magnitudes, $a_l, l = 1, 2, \ldots$, of these different components. Specifically, denoting by $\phi_j^{(l)}$ the jth element of the lth mode, the amplitudes a_l can be obtained by minimizing the representation error

$$\varepsilon = \sum_{n,j}\left[\tilde{X}_{n,j} - \sum_l a_l \phi_j^{(l)} g_l(n\Delta t)\right]^2, \tag{26}$$

where $\tilde{X}_{n,j}$ is the jth component of the response vector at time $n\Delta t$, and $g_l(t)$ represents the free response of the lth mode at time t which is a linear combination of the functions

$$g_{ls}(t) = \exp(-\zeta_l\omega_l t)\sin(\omega_l\sqrt{1-\zeta_l^2}\, t), \tag{27a}$$

$$g_{lc}(t) = \exp(-\zeta_l\omega_l t)\cos(\omega_l\sqrt{1-\zeta_l^2}\, t). \tag{27b}$$

3. COMPUTATIONAL ASPECTS

The solution of the convection step is obtained through a time domain boundary element method for unsteady flows as proposed by Yao *et al.* (1989) and Yao & Liu (1994). The potential flow field is solved by an extended high-order boundary element method derived from a modified Morino scheme. Details of the scheme are given by Morino (1974), Morino & Kuo (1974), Bristow (1997) and Shen & Proft (1980). However, the scheme used in the present study is based on that developed by Shen & Proft (1980). In the present approach, a high-order boundary element method which uses cubic spline curved panels and linear source and vorticity distributions (Shen & Proft 1980) is adopted. The vortical motion is governed by an Euler-type equation which is solved in a Lagrangian domain. A number of discrete vortex tracking techniques in the Lagrangian frame have been proposed by such researchers as Giesing (1968), Chorin (1973), Basu & Hancock (1978), Chow & Huang (1985), Kim & Mook (1986), and Lee & Smith (1987). These techniques are adopted for the handling of the travelling vortices and the wake and their interaction with the blades. The diffusion step of the solution is obtained by considering the turbulent diffusion of the vortex core. If the path of the vortex is assumed to be unaffected by viscous effects in the lowest order, then Lamb's (1932) viscous core vortex model can be used to simulate turbulent diffusion within the vortex.

However, in this case, the viscosity in Lamb's model is replaced by ν_t the eddy diffusivity of the turbulent flow.

The determination of the structural response starts by the computation of the aerodynamic forces and moment according to equations (12) and (13), where the integrals are performed numerically using a Gaussian quadrature (Carnahan *et al.* 1969). Then, the dynamic response of the blades can be determined by numerically solving equations (8a) and (8b). Specifically, the system of second-order nonlinear equations (8) is first transformed into a system of nonlinear first-order equations

$$\frac{\mathrm{d}\mathbf{Y}_k}{\mathrm{d}t} = \mathbf{F}[t,\, Y_k(1),\, Y_k(2),\, Y_k(3),\, Y_k(4)], \tag{28}$$

where

$$Y_k(1) = h(k\Delta t),\; Y_k(2) = \dot{h}(k\Delta t),\; Y_k(3) = \theta(k\Delta t), \quad \text{and} \quad Y_k(4) = \dot{\theta}(k\Delta t) \tag{29}$$

For each time step, equation (28) is integrated using different predictor-corrector methods according to the accuracy required. For example, if a second-order accuracy, $\mathcal{O}(\Delta t^2)$, is imposed, the corresponding formulae for the predictor and corrector are given by

$$\mathbf{Y}^0_{k+1} = \mathbf{Y}_k + \mathbf{F}[t_k,\, Y_k]\Delta t, \tag{30}$$

for the predictor step and

$$\mathbf{Y}^1_{k+1} = \mathbf{Y}_k + [\mathbf{F}[t_k,\, \mathbf{Y}_k] + \mathbf{F}[t_{k+1},\, Y^0_{k+1}]]\,\frac{\Delta t}{2}, \tag{31}$$

for the corrector step. A detailed description of this scheme is given by Rice (1993).

The fluid–structure interactions are calculated according to the scheme shown in Figure 2. At each time step, an estimate of the structural response is obtained by integrating the structural dynamics equations under the assumption that the aerodynamic loading is constant for the time step t_i to t_{i+1}. This estimate of the structural response is used to update the boundary conditions for the flow field calculations. Once the aerodynamic coefficients are estimated for the new time t_{i+1}, the variations of the right-hand function $\mathbf{F}$ in the system of equations (16) can be linearized. This assumption enables the calculation of the structural response which, in turn, yields a different surface pressure distribution and a new loading. The procedure is iterated according to Figure 2 until a prescribed precision on h and θ (10^{-6} relative error between successive iterations) is attained. Thus, the iteration at every time step allows the true flow-induced vibrations of the blades to be determined.

In terms of computational effort, the present formulation does not require excessive computer resources. For example, the calculations for the case of the NACA 0012 airfoil with 35 panels and 1000 time steps with $\Delta t = 0{\cdot}05$ take less than 1 min of CPU time in a RISC 6000 workstation. The time series thus obtained provide sufficient information for the proper identification of the modal frequencies and damping coefficients. For the typical 1000 sample time series mentioned above, the ARMA method takes approximately 2 min of CPU time to complete the analysis. The whole calculations therefore take a total of 3 min in a RISC 6000 workstation.

4. FLUTTER ANALYSIS

The free vibrations of a thin airfoil have recently been analysed by Hall (1994) by formulating the response of the entire system (airfoil and fluid) as a set of homogeneous linear differential equations. The natural frequencies and damping ratios of the airfoil in the presence of the fluid are determined by solving a linear eigenvalue problem. This problem is

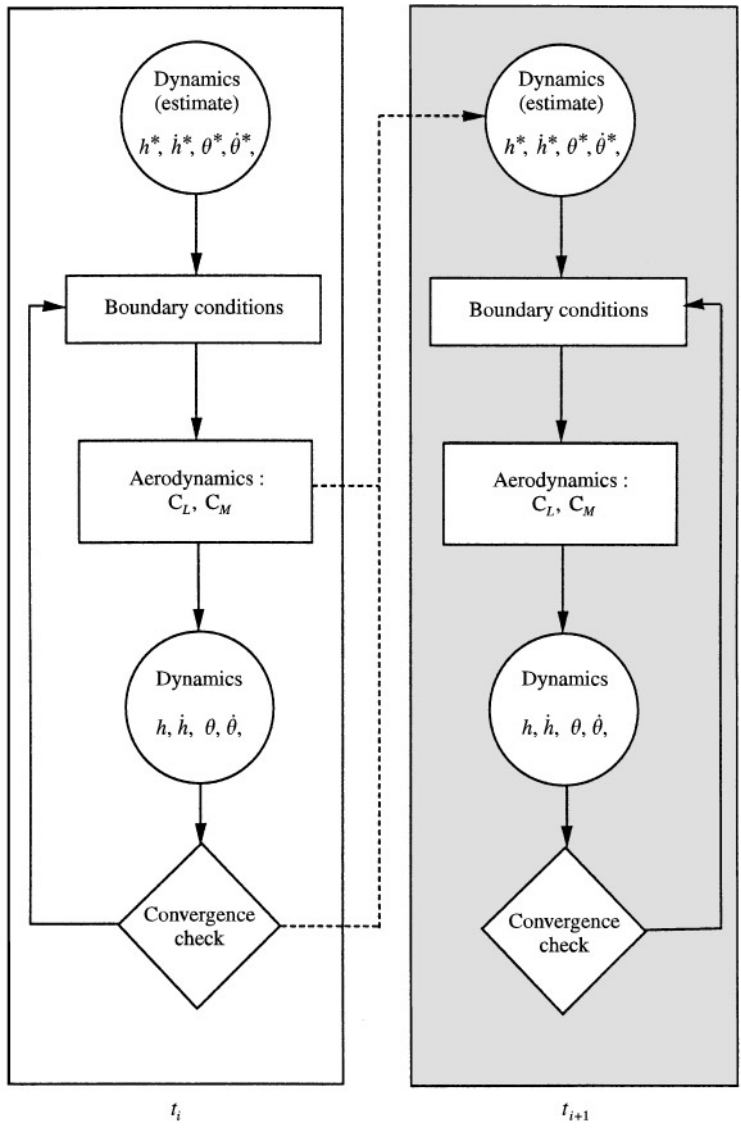

Figure 2. Integrated aerodynamics-structural dynamics flow chart.

reconsidered here, first to confirm the adequacy of the time-marching technique for the prediction of the natural frequencies and damping ratios of the structure as well as of the flutter speed, and then to investigate the effect of nonlinearities present in the aerodynamic and structural formulations on the response of the fluid–structure system.

To validate the accuracy of the time-marching strategy, and in particular of its time history analysis/identification component, it was decided to march in time the incremental relations derived by Hall and to compare the corresponding estimates of the natural frequencies (ω/ω_α) and damping ratios, $\mathscr{R}e(\lambda)$, with their counterparts obtained by Hall from the associated eigenvalue problem. The results of this comparison are depicted in Figures 3 and 4. In these figures, three sets of calculations are compared: (i) Hall's (1994) results, (ii) the results obtained by time-marching Hall's formulation (denoted as "Hall time

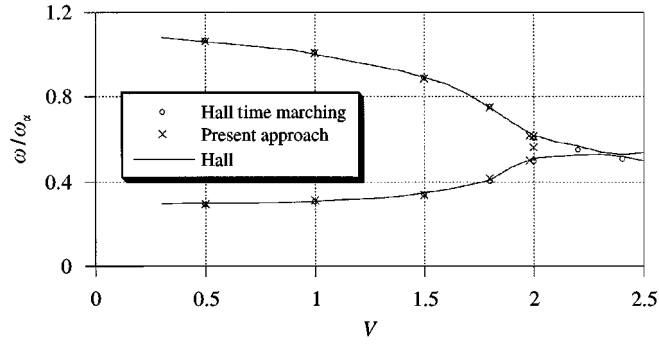

Figure 3. Comparison with Hall's (1994) frequency calculations; imaginary part of the eigenvalues.

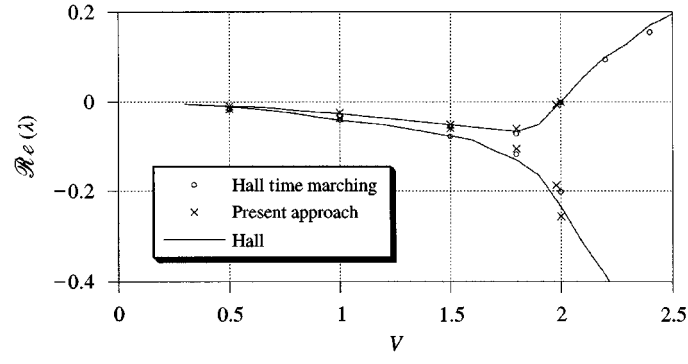

Figure 4. Camparison with Hall's (1994) damping ratio calculations; real part of the eigenvalues.

marching"), and (iii) the present time-marching results (designated as "Present"). The results for the Hall's case as well as the Hall time-marching case are for an inviscid fluid. On the other hand, the calculations using the present method are for a NACA 0012 airfoil with the structural model shown in Figure 1 and the following parameters: $\mathrm{Re} = \infty$, $m = 20{\cdot}0\,\mathrm{kg/m}$; $I = 1{\cdot}25\,\mathrm{kg\,m}$; $k_h = 1{\cdot}8\,\mathrm{N/m^2}$; $k_\theta = 1{\cdot}25\,\mathrm{N}$; $a = 0{\cdot}1\,\mathrm{m}$ and $c = 1\,\mathrm{m}$. These parameters are consistent with those considered by Hall (1994). The ω/ω_α and $\mathscr{R}e(\lambda)$ were obtained from an order 100 autoregressive model, AR(100), of the structural responses h, θ, C_L and C_M. This model accounts for 200 possible modes of response, two of which are required for the structural aspects of the problem. The large number of modes that can be used for the aerodynamic modelling (198) compares well with the 220 modes used by Hall.

Clearly, the agreement between the first two sets of curves is excellent at all speeds considered, thus indicating that the ARMA technique very accurately recovers the natural frequencies and damping ratios of the combined fluid–structure system. In this context, note further that the estimation of the characteristics of the highly damped mode near and past the flutter point is a very challenging identification problem since this mode disappears after only very few cycles and its frequency is very close to the dominant mode which is characterized by a very small, positive or negative, damping ratio. Notwithstanding these challenges, the ARMA technique also provides reliable estimates of the natural frequency and damping ratio of this overshadowed mode. Furthermore, it can be seen that the present results match very closely the values obtained by Hall (1994), thereby validating the present procedure.

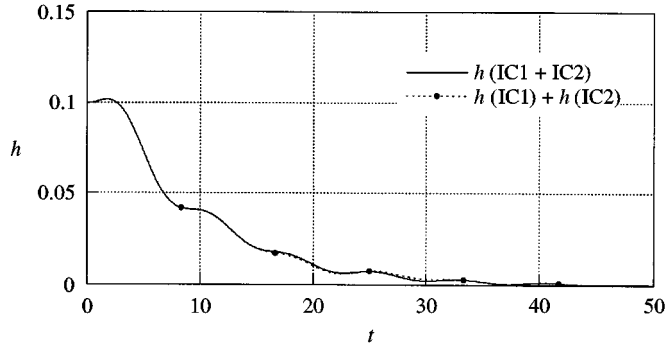

Figure 5. Linearity check at $V = 1{\cdot}8$ for the NACA 0012 airfoil.

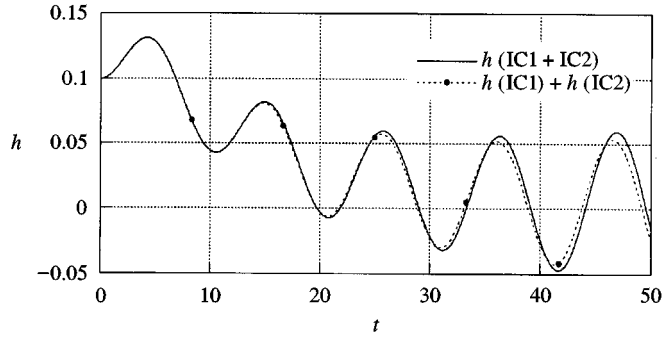

Figure 6. Linearity check at $V = 2{\cdot}02$ (flutter) for the NACA 0012 airfoil.

The existence/absence of nonlinear interactions in a system can be assessed from the time histories of its free response. Indeed, if the system is linear, its free response depends linearly on the initial conditions and the principle of superposition holds, i.e. the response to the set of initial conditions IC1 + IC2 is the sum of the responses obtained from initial conditions IC1 and IC2 computed separately. To remove any potential nonlinear effect arising from the trigonometric functions appearing in the structural dynamic equations of motion (8), the linear set of equations (9) have been used in the ensuing computations. The comparison suggested above is depicted in Figure 5, where the results were obtained using the present method, the linearized set of equations (9) and a dimensionless velocity $V = 1{\cdot}8$. The initial conditions IC1 and IC2 were defined as $\{h, \dot{h}, \theta, \dot{\theta}\} = \{0, 0, 0{\cdot}1, 0\}$ and $\{h, \dot{h}, \theta, \dot{\theta}\} = \{0{\cdot}1, 0, 0, 0\}$, respectively. No difference between the bending response corresponding to IC1 + IC2 and the sum of the displacements for IC1 and IC2 can be observed, thereby suggesting that the system is essentially linear. A second set of results were obtained at $V = 2{\cdot}02$, right above the flutter point, and is shown in Figure 6. Note that there is a slight discrepancy between the two curves. This implies that a small nonlinear effect is present.

To confirm the existence of nonlinearity in the fluid–structure system and to assess its characteristics, a comparison between the structural response obtained with initial conditions (IC1 + IC2)/10 and the sum of the displacements corresponding to IC1/10 and IC2/10, respectively, has been performed. The results of these computations (not shown here for brevity), which indicate that there is almost no discrepancy between the two curves, confirm the initial condition dependence and thus the nonlinearity of the system. Finally,

this improved matching at a reduced response level also demonstrates that the nonlinearity of the system can be attributed to powers larger than 1 of certain variables, so that a forced response of this system would be expected to display superharmonics of the excitation frequency.

The identification of the source of the nonlinear behaviour observed in Figure 6 was accomplished by performing a series of linearizations of the fluid governing equations, [Equations (4)–(6)], and the fluid–structure boundary condition (3). The structural equations of motion have already been linearized for the results shown in Figure 6. This effort revealed that although there are several nonlinear contributing terms, the discrepancy shown in Figure 6 comes almost exclusively from the fluid–structure coupling exhibited in the tangency condition (3). More specifically, the nonlinearity was observed to be associated with the presence of trigonometric functions of the time-varying angle of attack of the airfoil in both equation (3) and the system of equations yielding the strength of the source distributions on the airfoil (Yao *et al.* 1995). In fact, after linearizing these terms according to $\sin\alpha \approx \alpha$ and $\cos\alpha \approx 1$, an almost perfect match was found between the response associated with the initial conditions IC1 + IC2 and the sum of the responses corresponding to IC1 and IC2 computed separately (Figure 7).

It should be noted that the geometry of the airfoil seems to be of secondary importance, as suggested by the good agreement between the present investigation, based on a NACA 0012 airfoil, and Hall's (1994), based on a flat plate model. The increased level of interaction between the fluid and the structure that exists around the flutter speed can also be noted from the wake path and structure. Indeed, shown in Figures 8 and 9 are the vortex wake

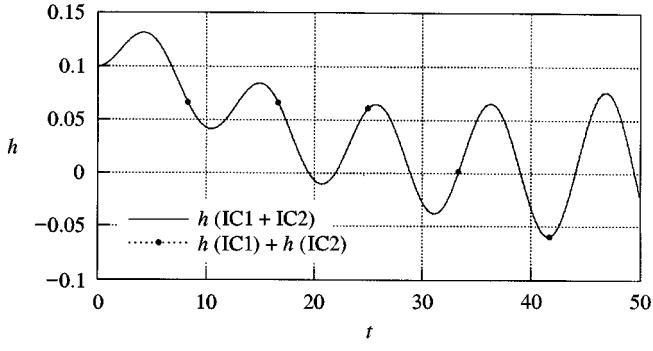

Figure 7. Linearity check at $V = 2{\cdot}02$ (flutter) with linearized boundary conditions for the NACA 0012 airfoil.

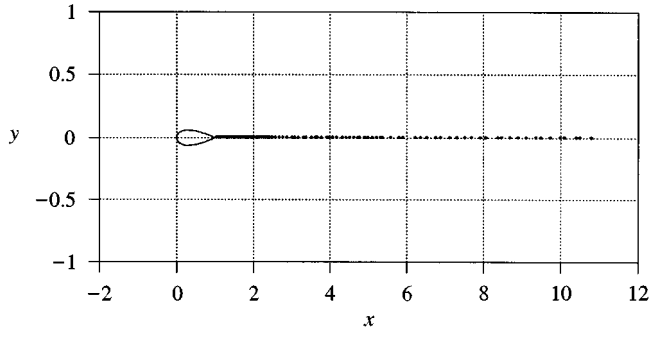

Figure 8. Wake configuration ($t = 300$) at $V = 1{\cdot}8$ for the NACA 0012 airfoil.

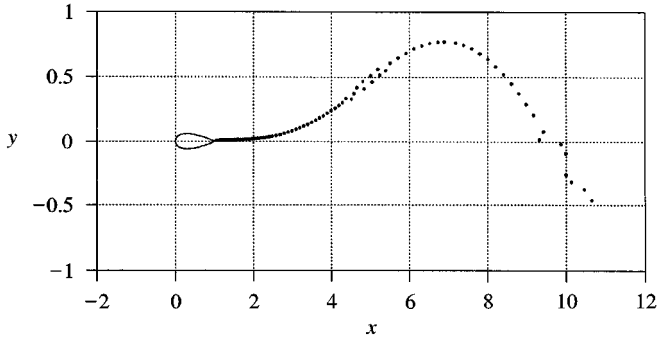

Figure 9. Wake configuration ($t = 300$) at $V = 2{\cdot}0$ for the NACA 0012 airfoil.

structures obtained at time $t = 300$ at the dimensionless velocities $V = 1{\cdot}8$ and $V = 2{\cdot}0$. Note the almost perfect straight line trajectory of the vortices obtained below flutter (Figure 8). At the flutter speed ($V = 2{\cdot}0$), however, the fluid–structure system resonates and all of its characteristics exhibit undamped oscillations, as confirmed in Figure 9 for the wake. This result is in sharp contrast with classical flutter analyses that prescribe a straight line wake in all flow conditions. The correct prediction of the vortex path is of course of primary importance if the response of another structure located downstream of the airfoil is to be predicted, as encountered for example in turbomachinery applications.

The effect of Re, or in this case, turbulent diffusivity, on the fluid-structure interactions is assessed next. Additional calculations using the present method were carried out assuming Re = 10,000, 1000, 300, 200 and 100. The parameters used for these calculations are identical to Hall's case at $V = 1{\cdot}8$ with initial conditions given by IC1 + IC2. These calculations are compared with the results shown in Figure 3 and 4 for $\mathrm{Re} = \infty$ and are plotted in Figure 10. Parts (a) and (b) of Figure 10 show the bending and pitching deformation histories. At $V = 1{\cdot}8$, Hall (1994) predicted a negative damping. This finding is also realized when the present method is used to carry out the calculations assuming $\mathrm{Re} = \infty$ (potential flow), or a non-diffusive vortex core. The results of the $\mathscr{R}e(\lambda)$ and the ω/ω_α ratio for all Re calculated are listed in Table 1. It can be seen that reducing Re leads to a decrease in damping; i.e., the $\mathscr{R}e(\lambda)$ goes from negative to positive. In other words, a decrease of Re destabilizes the fluid–structure system. Part (c) of Figure 10 shows the behaviour of the downwash, w/w_0 (normalized by the potential flow value) generated by a diffusive vortex travelling from the trailing edge of the airfoil at freestream velocity. These results show that a diffusive core generates a different induced velocity field behind the airfoil, which in turn modifies the aerodynamic damping properties.

In order to explain the relationship between aerodynamic damping and Re, it is probably best to start from Wagner's function, which describes the response of an airfoil to a step function input. This response is known to be gradual in contrast with the response computed under the quasi-steady assumption with a similar step function input. The difference between the two models is given by the presence/absence of flow-propagated vortices generated at the trailing edge, which represent the flow memory. Wagner's function is characteristic of the calculations shown in Figure 10 under the potential flow assumption, or $\mathrm{Re} = \infty$. In this case, the vortices do not diffuse and the wake is propagated to downstream infinity. The quasi-steady situation corresponds to the limiting case of $\mathrm{Re} = 0$, where the diffusivity of the vortices is so large that they disappear immediately after

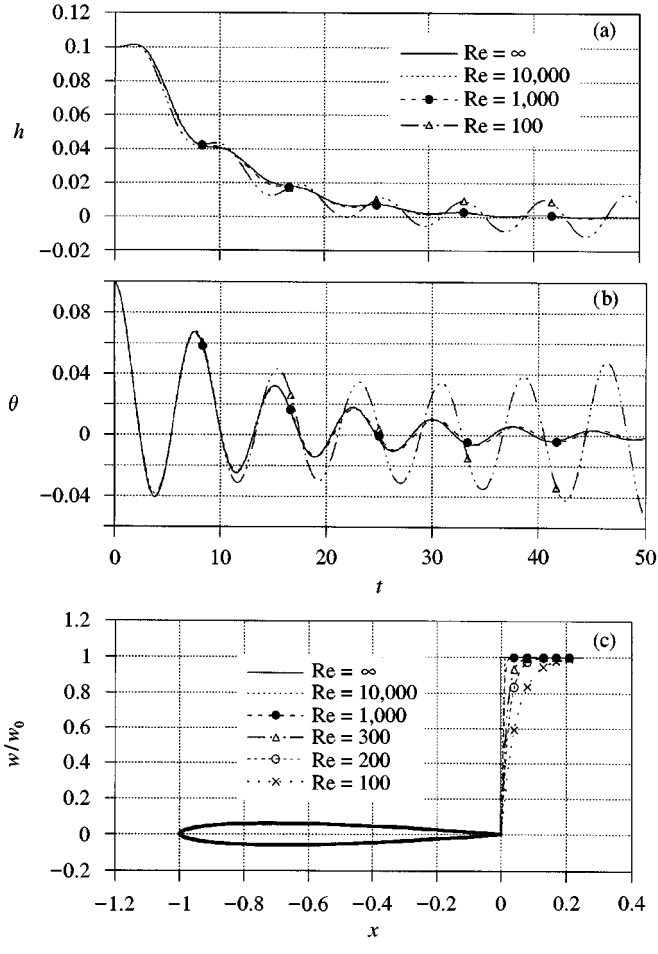

Figure 10. Reynolds number effects on (a, b) structural vibrations and (c) wake behaviour at $V = 1{\cdot}8$ for the NACA 0012 airfoil.

TABLE 1

Variation of the $\mathscr{R}e(\lambda)$ and the ω/ω_α ratio with Re for the NACA 0012 airfoil at $V = 1{\cdot}8$

Re	$\mathscr{R}e(\lambda)$	ω/ω_α
∞	− 0·064	0·758
10000	− 0·064	0·748
1000	− 0·053	0·736
300	− 0·017	0·732
200	+ 0·015	0·728
100	+ 0·047	0·727

leaving the trailing edge. In other words, no wake is present and the flow cannot "remember" what happened at previous time moments. It can be seen that the presence of the wake leads to a lag in the response which is in fact the aerodynamic damping. Therefore,

it can be deduced from Figure 10(c) that as Re is decreased, the effect of the wake is diminished over an increasingly larger area. This leads to a local "amnesia" of the flow, which approaches the undamped instantaneous response characteristic of the quasi-steady flow assumption. Thus, at lower Re, the response of an airfoil to a step function becomes less damped.

5. PREDICTIONS OF LIMIT CYCLE OSCILLATIONS (LCO)

The time marching of both the fluid and structural dynamic equations allows not only the determination of the flutter speed but also permits the prediction of the post-flutter behaviour of the system; in particular, the source of nonlinearity in the post-flutter regime. Also, it is possible to examine whether the response will grow in time until a steady-state behaviour is reached and to determine the amplitudes of the corresponding limit-cycle oscillations (LCO). Furthermore, the present technique allows the consideration of nonlinearity in the response of the structure as encountered, for example, in connection with dry friction (stick-slip) mechanisms and/or the presence of gaps (free play) or discontinuous contacts, e.g. shroud contact in turbomachine blades. In order to illustrate these points, four cases that simulate these situations approximately are considered. The results and insights thus gained from the analysis are discussed below.

Case (*a*). As a first test of the capabilities of the present method, the response of the structural system shown in Figure 1 with the nonlinear equations of motion given by equations (8a, b) was investigated just above the flutter speed ($V = 2{\cdot}02$). Shown in Figure 11 are the response time history of bending (plunging) deflection (h versus t) and the corresponding phase plane plot ($\dot{h}$ versus h) which clearly indicate that the amplitude of the oscillations reaches a steady state level at a dimensionless time $t \approx 200$. The limit cycle is seen to be very close to a pure circle, demonstrating that flutter occurs only along one mode and that the harmonics of the fundamental frequency are not significantly present in the response. In fact, an ARMA analysis of the time histories of the response shows the existence of small but detectable second, third, and higher harmonics which are clearly associated with the cosine and sine terms discussed in the foregoing. Note that a totally analogous situation is observed in connection with the torsional (pitching) response angle θ. For brevity, the results are not shown.

Case (*a′*). A further attempt to identify the source of nonlinearity is to repeat the calculations of Case (a) using the linear set of structural dynamic equations (9a, b). Thus, there are no nonlinearities introduced by the airfoil structure and any nonlinearities shown in the results can be attributed to those deriving from the fluid–structure interactions. Again, the calculations were carried out with $V = 2{\cdot}02$, just above the flutter speed. The results for h and $\mathrm{d}h/\mathrm{d}t$ are shown in Figure 12. It can be seen that a circular LCO is again obtained, thus indicating that flutter occurs only along one mode and that the harmonics of the fundamental frequency are not significantly present in the response. Furthermore, the amplitude level of h has only slightly increased, by approximately 20%, thereby demonstrating that, in the fluid–structure system, the strongest nonlinearity is in fact derived from the fluid–structure interactions and not from the structure. Further evidence in support of this conclusion can be seen from a comparison of the time histories of θ for Cases (a) and (a′). These are shown in Figure 13. It is seen that both traces approach a LCO behaviour; however, consistent with the results of the bending deformation analysis, it is found that the amplitude of θ for Case (a′) is higher than that of Case (a), thus indicating that structural nonlinearities further damped the amplitudes of the oscillations.

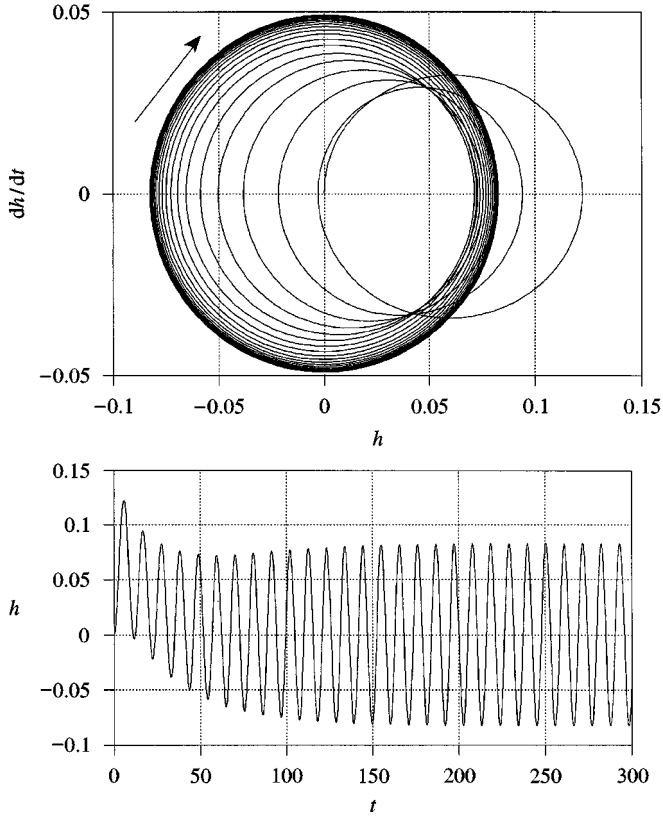

Figure 11. LCO for Case (a) : bending response.

Case (*b*). The response of nonlinear structural systems to the oncoming flow has been studied on the basis of the modified equations of motion

$$m\ddot{h} - ma\cos\theta\ \ddot{\theta} + k_h h + ma\sin\theta\ \dot{\theta}^2 + F_h = L, \tag{32a}$$

$$I\ddot{\theta} - ma\cos\theta\ \ddot{h} + k_\theta \theta + F_\theta = M, \tag{32b}$$

where F_h and F_θ are nonlinear functions of h, θ, and their first derivatives. The values of the parameters m, a, I, k_h and k_θ were kept the same as in the previous numerical results. The potential effects of a rub (dry friction) between the airfoil and another structure, that are at rest separated by gaps h_0 and θ_0, were investigated by introducing the nonlinear terms

$$F_h = \begin{cases} \mu_h\sqrt{k_h m}V\ \mathrm{sgn}(\dot{h}), & h > h_0 \\ 0, & -h_0 \le h \le h_0 \\ -\mu_h\sqrt{k_h m}V\ \mathrm{sgn}(\dot{h}), & h < -h_0, \end{cases} \tag{33a}$$

$$F_\theta = \begin{cases} \mu_\theta\sqrt{k_\theta I}(V/c)\ \mathrm{sgn}(\dot{\theta}), & \theta > \theta_0 \\ 0, & -\theta_0 \le \theta \le \theta_0 \\ -\mu_\theta\sqrt{k_\theta I}(V/c)\ \mathrm{sgn}(\dot{\theta}), & \theta < -\theta_0, \end{cases} \tag{33b}$$

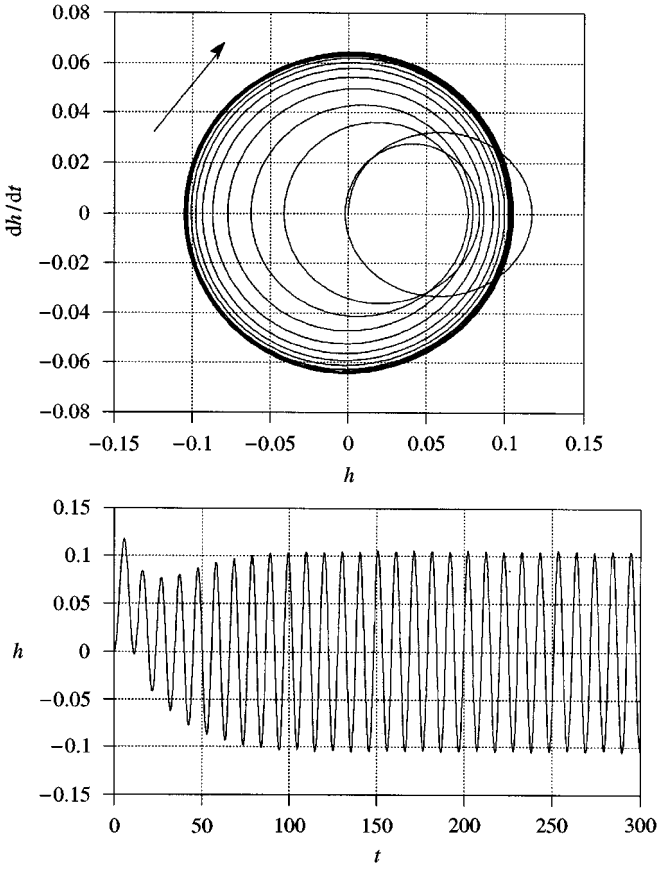

Figure 12. LCO for Case (a′) : bending response.

where the parameters μ_h and μ_θ are the dimensionless coefficients of friction associated with the bending and torsional motions, respectively. To exemplify the effects of such a nonlinear damping mechanism, the values $h_0 = 0{\cdot}03c$, $\theta_0 = 0{\cdot}06$, $\mu_h = 0{\cdot}0015$ and $\mu_\theta = 0{\cdot}002$ were selected and the response of the fluid/structure system was computed until time $t = 300$. Shown in Figure 14 are the response time history of the bending deflection and the corresponding phase-plane plot. These figures again indicate the rapid convergence of the response of the system to a limit-cycle oscillation of magnitude approximately 40% smaller than the one exhibited by the original system (Figure 11). This reduction of the amplitude of response has de-emphasized the role of second, third and higher harmonics of the response, which are associated with the trigonometric functions of the angle of attack, as discussed above, and are of aerodynamic origin. However, the symmetrical nonlinearity of the structural behaviour specified by equations (33a, b) yields a significant contribution of all odd harmonics the presence of which has been confirmed by an ARMA analysis of the response time histories.

Case (*c*). As a final example of structural nonlinearity, it was assumed that the structure is undamped but is characterized by a bilinear stiffening behaviour. That is, the model is of the form of equations (8) with stiffnesses k_h and k_θ that vary with the amplitude of response. Such governing equations can be written in the form of equation (29)

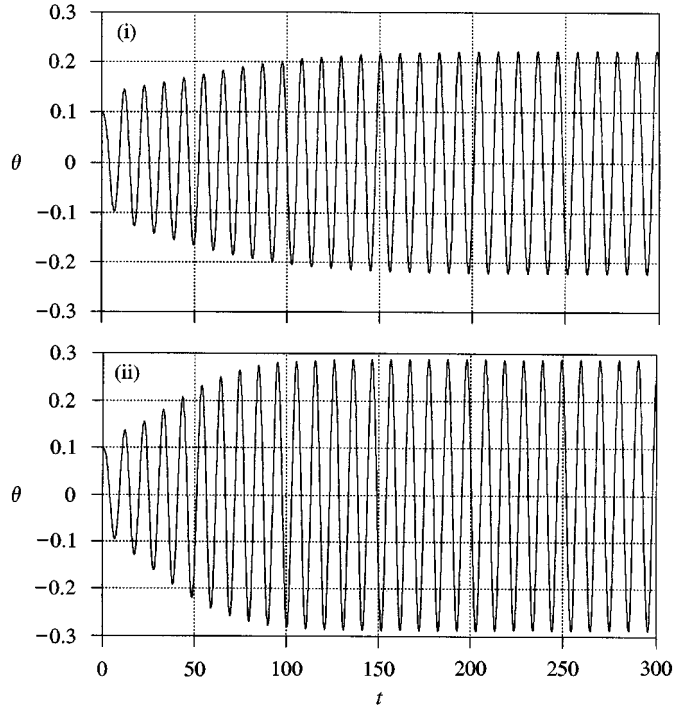

Figure 13. θ time history for (i) Case (a) and (ii) Case (a′).

with

$$F_h = \begin{cases} (k'_h - k_h)(h - h_0), & h > h_0 \\ 0, & -h_0 \le h \le h_0 \\ (k'_h - k_h)(h + h_0), & h < -h_0, \end{cases} \tag{34a}$$

$$F_\theta = \begin{cases} (k'_\theta - k_\theta)(\theta - \theta_0), & \theta > \theta_0 \\ 0, & -\theta_0 \le \theta \le \theta_0 \\ (k'_\theta - k_\theta)(\theta + \theta_0), & \theta < -\theta_0, \end{cases} \tag{34b}$$

where h_0 and θ_0 are the threshold values at which the bending and torsional stiffnesses change. To exemplify the effects of such a structural nonlinearity, the high-amplitude additional stiffnesses k'_h and k'_θ were selected to be 15 and 5%, respectively, larger than their low amplitude counterparts k_h and k_θ, corresponding to the "soft system", which were set to their prior values in Cases (a) and (b). Further, the threshold values were chosen as $h_0 = 0{\cdot}03c$ and $\theta_0 = 0{\cdot}06$ and the velocity of the oncoming flow was selected to be the same as before ($V = 2{\cdot}02$), slightly above the flutter point.

Shown in Figure 15 are the response time history of the bending deflection and the corresponding phase plane plot which reveal, as in the other two cases, that the system reaches a steady-state situation. Note, however, that the amplitude of these limit cycle oscillations is approximately half of its corresponding value for the original system. In fact, it can be seen from Figure 15 that the bending deformation, h, barely exceeds the threshold

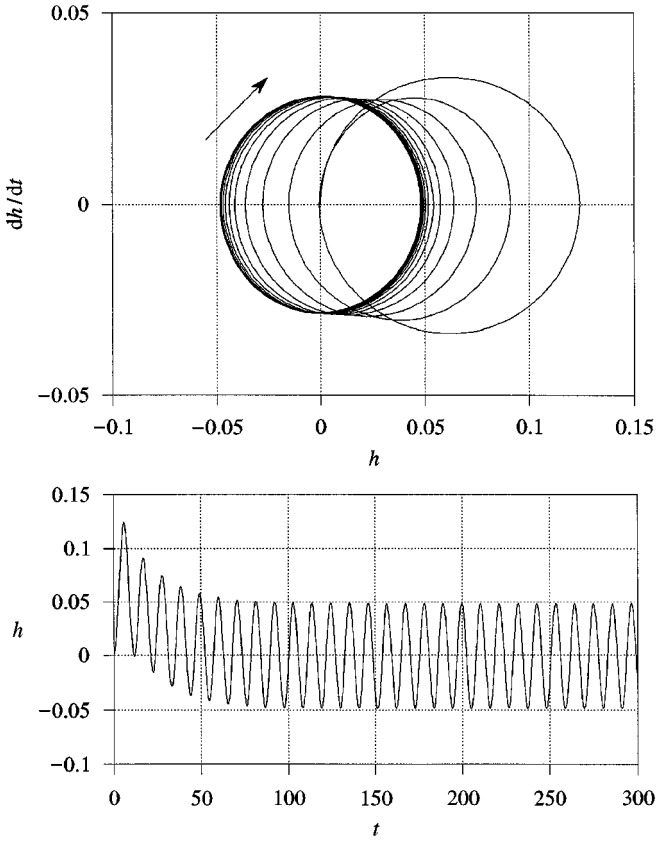

Figure 14. LCO for Case (b) : bending response.

value h_0. Since a similar situation is encountered in connection with the torsional response, $\theta(t)$, it is concluded that the change of stiffness physically limits the response to amplitudes that are only slightly larger than the threshold values h_0 and θ_0.

This behaviour can be understood as follows. As shown in Figure 15, the initial values of h and θ are below their corresponding thresholds. Since the flow velocity is above the flutter speed for the "soft system", its response will increase with time until the amplitude of response exceeds the threshold values. At this point, the system switches to "stiff" and the flutter speed becomes higher than the existing freestream velocity. The ensuing response will then consist of damped exponentials as seen in Figure 5, and will rapidly fall below the threshold values. In this manner, the maximum amplitude reached by the system can only be slightly above the threshold at which the system switches from "soft" to "stiff", as observed in Figure 15.

The important changes in the magnitudes of the limit cycle oscillations (compare Figures 14 and 15 with Figure 11) when only small nonlinear effects are introduced in the structural model of the system may shed some light on the difficulties encountered in some investigations (Meijer & Cunningham 1995) in predicting accurately the amplitude of the limit cycle oscillations on the basis of a purely aerodynamic nonlinearity.

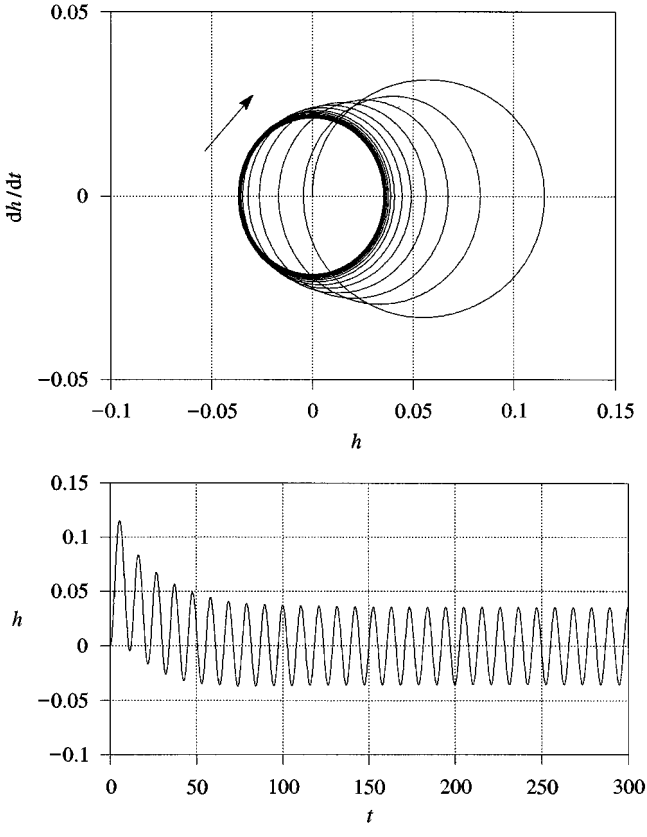

Figure 15. LCO for Case (c) : bending response.

6. CONCLUSIONS

In this paper, a complete methodology for the analysis of flow-induced vibrations has been presented. This approach included five specific elements: (i) the modelling of the fluid, (ii) the prediction of the dynamic response of the structure, (iii) the specification of the coupling between the fluid and the structure, (iv) the frequency domain analysis of the response time histories, and (v) the assessment of the potential for failure. Computational strategies to accomplish the first four tasks have been presented in detail. This paper concentrates more specifically on flow-induced vibrations encountered in a single blade/airfoil. Application of these techniques to investigate the free vibration and flutter speed determination of a single blade/airfoil has been carried out. Specifically, the following results have been obtained.

(a) The nonlinear character of the fluid–structure interactions associated in particular with the flow tangency condition is properly accounted for and produces significant changes in the response of the system in the neighbourhood of the flutter speed but appears to have only a small effect below this value. Similarly, the path of the wake shed from the airfoil is found to have a definite curvature when the flow velocity is comparable to the flutter speed but not at lower regimes.

(b) The fully nonlinear character of the analysis performed permits the prediction of the post-flutter behaviour of the system, including the existence and amplitudes of limit-cycle oscillations for both linear and nonlinear structural models of the airfoil. In this regard, it

was observed that the inclusion of small nonlinear terms in the description of the structure can lead to large changes in the amplitudes of the limit cycle oscillations. This result demonstrates the importance of properly accounting for such phenomena as free play, rub between parts, and possible stick-slip mechanisms in the structural modelling.

(c) The ability to resolve these characteristics depends, to a great extent, on the time-series analysis technique employed. It is shown that the conventional FFT method is not appropriate but that an alternative approach based on autoregressive moving-average (ARMA) discrete systems performs extremely well.

(d) The time-marching technique is able to account for the fluid-structure interaction effects properly, including the interactions between the oncoming flow, the structure and the wake shed by the structure. Therefore, it is very suitable for the analysis of the general class of flow-induced vibration problems.

ACKNOWLEDGEMENTS

Contract support given to R.M.C.So during his tenure at Arizona State University by the Naval Surface Warfare Center, Carderock Division, Department of the Navy, Bethesda, MD 20084, U.S.A., is gratefully acknowledged. The contract was monitored by Dr W. Tang. R.M.C.So would further like to acknowledge the support given to him by the Hong Kong Polytechnic University for the completion of the project and the preparation of this paper.

REFERENCES

BASU, B. C. & HANCOCK, G. J. 1978 The unsteady motion of a two-dimensional airfoil in incompressible inviscid flow. *Journal of Fluid Mechanics* **87,** 159–178.

BÉLANGER, F., PAÏDOUSSIS, M. P. & DE LANGRE, E. 1995 Time-marching analysis of fluid-coupled systems with large added mass. *AIAA Journal* **33,** 752–757.

BRISTOW, D. R. 1977 Recent improvements in singularity methods for the flow field analysis about two-dimensional airfoils. AIAA Paper 77–641.

CARNAHAN, B., LUTHER, H. A. & WILKES, J. O. 1966 *Applied Numerical Methods*. New York: Wiley.

CHIANG, H.-W. D. & KIELB, R. E. 1993 An analysis system for blade forced response. *ASME Journal of Turbomachinery* **115,** 762–772.

CHORIN, A. J. 1973 Numerical study of slightly viscous flow. *Journal of Fluid Mechanics* **57,** 785–796.

CHOW, C. Y. & HUANG, M. K. 1985 Unsteady flows about a Joukowski airfoil in the presence of moving vortices. AIAA Paper 85-0203.

FLEETER, S. 1994 Forced response unsteady aerodynamic experiments. *International Journal of Turbo and Jet Engines* **11,** 177–192.

GIESING, J. P. 1968 Nonlinear two-dimensional unsteady potential flow with lift. *Journal of Aircraft* **5,** 135–143.

HALL, K. C. 1994 Eigenanalysis of unsteady flows about airfoils, cascades, and wings. *AIAA Journal* **32,** 2426–2432.

JONES, K. D. & PLATZER, M. F. 1996 Time-domain analysis of low-speed airfoil flutter. *AIAA Journal* **34,** 1027–1033.

KEMP, N. H. & SEARS, W. R. 1955 The unsteady forces due to viscous wakes in turbomachines. *Journal of Aeronautical Sciences* **22,** 478–483.

KIM, M. J. & MOOK, D. T. 1986 Application of continuous vorticity panels to general unsteady incompressible two-dimensional lifting flows. *Journal of Aircraft* **23,** 464–471.

LAMB, S. H. 1932 *Hydrodynamics*, 6th edition. Cambridge: Cambridge University Press.

LEE, D. J. & SMITH, C. A. 1987 Distortion of the vortex core during blade/vortex interaction. AIAA Paper 87-1243.

MAJJIGI, R. K. & GLIEBE, PR. 1984 Development of a rotor wake/vortex model. NASA-CR-174849.

MARPLE Jr., S. L. 1987 *Digital Spectral Analysis with Applications*. Englewood Cliffs, NJ: Prentice-Hall.

MEIJER, J. J. & CUNNINGHAM Jr., A. M. 1995 Outline and applications of a semi-empirical method for predicting transonic limit cycle oscillation characteristics of fighter aircraft. *International Forum on Aeroelasticity and Structural Dynamics*, Manchester, U.K., 26–27 June, Vol. 2. Paper 75.

MIGNOLET, M. P. & RED-HORSE, J. R. 1994 ARMAX identification of vibrating structures: model and model order

determination. *Proceedings of the 35th Structures, Structural Dynamics, and Materials Conference*, Hilton Head, South Carolina, U.S.A. 18–20 April, pp. 1628–1637.

MORINO, L. 1974 A general theory of unsteady compressible potential aerodynamics. NASA CR-2464.

MORINO, L. & KUO, C. C. 1974 Subsonic potential aerodynamics for complex configurations — a general theory. *AIAA Journal* **12,** 191–197.

RICE, J. R. 1993 *Numerical Methods, Software, and Analysis*. London: Academic Press.

SHEN, C. C. & PROFT, E. 1980 An accurate method for calculation of potential flows about arbitrary airfoils. Northrop Corporation. Report No. NOR 80-174.

WEAVER, M. M. & FLEETER, S. 1994 Turbine Rotor Generated Forcing Functions for Flow Induced Vibrations. *International Journal of Turbo and Jet Engines* **11,** 139–161.

YAO, Z. X., JADIC, I., SO, R. M. C., LIU, D. D. & TANG, W. 1995 Flow-induced vibrations on a turbine blade in a blade row using a vortex dynamics model. Presented at the *International Forum on Aeroelasticity and Structural Dynamics*, 26–27 June, Manchester, U.K.

YAO, Z. X. & LIU, D. D. 1994 Vortex dynamics of blade-blade interaction. AIAA Paper 94-0737.

YAO, Z. X., GARCIA-FOGEDA, P., LIU, D. D. & SHEN, G. 1989 Vortex/wake flow studies for airfoils in unsteady motions. AIAA Paper 89-2225.